Human ISWI chromatin-remodeling complexes sample nucleosomes via transient binding reactions and become immobilized at active sites

Fabian Erdel[a], Thomas Schubert[b], Caroline Marth[a], Gernot Längst[b], and Karsten Rippe[a,1]

[a]Research Group Genome Organization and Function, Deutsches Krebsforschungszentrum and BioQuant, 69120 Heidelberg, Germany; and [b]Biochemie III, Universität Regensburg, 93053 Regensburg, Germany

Edited* by Peter H. von Hippel, Institute of Molecular Biology, Eugene, OR, and approved September 28, 2010 (received for review April 1, 2010)

Chromatin remodeling complexes can translocate nucleosomes along the DNA in an ATP-dependent manner. Here, we studied autofluorescent protein constructs of the human ISWI family members Snf2H, Snf2L, the catalytically inactive Snf2L+13 splice variant, and the accessory Acf1 subunit in living human and mouse cells by fluorescence microscopy/spectroscopy. Except for Snf2L, which was not detected in the U2OS cell line, the endogenous ISWI proteins were abundant at nuclear concentrations between 0.14 and 0.83 μM. A protein interaction analysis showed the association of multimeric Snf2H and Acf1 into a heterotetramer or higher-order ACF complex. During the G1/2 cell cycle phase, Snf2H and Snf2L displayed average residence times <150 ms in the chromatin-bound state. The comparison of active and inactive Snf2H/Snf2L indicated that an immobilized fraction potentially involved in active chromatin remodeling comprised only 1–3%. This fraction was largely increased at replication foci in S phase or at DNA repair sites. To rationalize these findings we propose that ISWI remodelers operate via a "continuous sampling" mechanism: The propensity of nucleosomes to be translocated is continuously tested in transient binding reactions. Most of these encounters are unproductive and efficient remodeling requires an increased binding affinity to chromatin. Due to the relatively high intranuclear remodeler concentrations cellular response times for repositioning a given nucleosome were calculated to be in the range of tens of seconds to minutes.

nucleosome translocation | fluorescence recovery after photobleaching | fluorescence correlation spectroscopy

Chromatin structure is a key determinant of gene regulation. The wrapping of the DNA around the histone octamer protein core in the nucleosome impedes the access of transcription factors to the DNA sequence information. Thus, changes of nucleosome positions at promoter and enhancer regions may directly affect gene expression (1–4). To control nucleosome positions (and with it the access to the associated DNA), a complex chromatin remodeling machinery operates in the eukaryotic cell nucleus. It comprises numerous different types of molecular machines that can translocate nucleosomes in an ATP-dependent manner. Chromatin remodelers can associate with different subunits to form remodeling complexes with distinct biological functions. Due to the high combinatorial complexity it is estimated that several hundreds of different chromatin remodeling complexes exist in humans. These comprise several groups of ATPases classified into the Snf2, ISWI, Mi-2, Chd1, Ino80, ERCC6, ALC1, CHD7, Swr1, RAD54, and Lsh subfamilies (5–7). The associated subunits are responsible for the targeting of the remodeling complexes as well as for the regulation of the remodeling activity (6, 8). One of the best conserved ATPase families involved in chromatin remodeling is the ISWI family (9). It consists of two ATPases, Snf2H and Snf2L in humans. All ISWI proteins contain a conserved ATPase domain that belongs to the superfamily of DEAD/H-helicases (10, 11), located in the N-terminal half of the proteins. Substrate recognition and catalysis are coupled via a SANT and a SLIDE domain near the C terminus that mediate binding to DNA and histone tails (12, 13). ISWI family complexes have various functions, including chromatin assembly and nucleosome spacing (ACF, CHRAC, and RSF), replication (WICH), transcriptional repression (NoRC), and transcriptional activation (NURF and CERF) (14–17). Thus, it seems likely that the accessory proteins present in a given complex regulate its function and are important for target recognition.

Although the ISWI-type chromatin remodelers have been extensively studied in vitro, an analysis in living cells is currently missing. Here, we present a study on the mobility and interactions of chromatin remodeling complexes in living cells. Autofluorescent protein constructs of human Snf2H, Snf2L, Snf2L +13, and Acf1 were investigated in human osteosarcoma and murine fibroblast cell lines. Their intracellular localization as well as their dynamic behavior was analyzed using a multiscale fluorescence fluctuation microscopy approach that comprised noninvasive fluorescence recovery after photobleaching (FRAP), continuous photobleaching (CP), and fluorescence (cross-)correlation spectroscopy (FCS/FCCS)-based experiments (18–21). The results from our quantitative analysis are rationalized in terms of a "continuous sampling" mechanism: In G1/2 phase of the cell cycle, all nucleosomes are probed by a given remodeling complex within minutes via transient binding reactions but only a small fraction of these binding events leads to repositioning. In contrast, extensive repositioning occurs at replication foci in S phase or at DNA repair sites.

Results

Snf2H-GFP and GFP-Snf2L Are Catalytically Active and Bind to Chromatin. GFP-tagged Snf2H, Snf2L, and Acf1 proteins were transfected into human U2OS cells and murine NIH 3T3 cells. As expected, the proteins were localized to the nucleus in both cell lines (Fig. 1, Fig. S1). As a cell cycle marker the proliferating cell nuclear antigen fused to a red fluorescent protein domain (PCNA-RFP) was cotransfected. PCNA is a central component of the replication machinery and shows a characteristic punctuate pattern during S phase (22). In mouse NIH 3T3 cells, which display distinct DNA dense pericentric heterochromatin foci, the remodeler concentration increased with the DNA density. This increase visualizes the chromatin binding of the GFP-tagged remodelers, in agreement with previous findings from Varga-Weisz and colleagues who characterized the intranuclear localization of Snf2H and its associated Acf1 subunit by immunostaining in mouse cells (23). The ratio between the DAPI or histone H2A-RFP fluorescence signal and GFP-tagged Snf2H/Snf2L/Snf2L+13/Acf1 was similar throughout the cell nuclei in the NIH 3T3 cell line (Fig. S1). This observation indicates a rather homogenous distribution of bound remodeling complexes on the nucleosome chain at the given resolution during G1/2 phase. The inactive

Author contributions: F.E., G.L., and K.R. designed research; F.E., T.S., and C.M. performed research; F.E. analyzed data; and F.E., G.L., and K.R. wrote the paper.

The authors declare no conflict of interest.

*This Direct Submission article had a prearranged editor.

[1]To whom correspondence should be addressed. E-mail: karsten.rippe@dkfz.de.

This article contains supporting information online at www.pnas.org/lookup/suppl/doi:10.1073/pnas.1003438107/-/DCSupplemental.

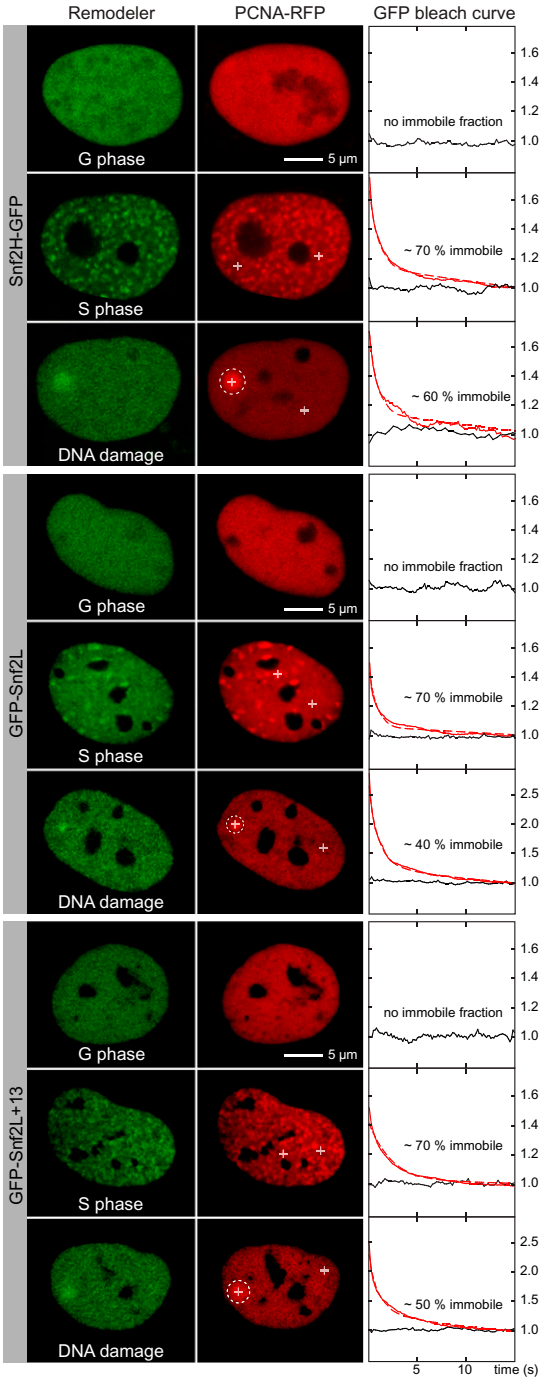

Fig. 1. Confocal images of Snf2H-GFP, GFP-Snf2L, and GFP-Snf2L+13 in U2OS cells. For each protein G1/2 phase (*Top*), S phase (*Middle*), and the case of DNA damage (*Bottom*) are shown. Immobilization at replication foci in S phase and at DNA repair sites is evaluated from the decay of the CP curves depicted in red compared with the black curves measured at regions of low PCNA density.

variant GFP-Snf2L+13, which contains exon 13 disrupting the enzyme's ATPase cassette (24), displayed the same localization as GFP-Snf2L, demonstrating that chromatin binding was independent of ATPase activity. Interestingly, the ratio of remodeler to chromatin concentration was reduced at some heterochromatin foci in NIH 3T3 cells (arrows in Fig. S1). This finding points to the partial exclusion of remodelers from these sites, consistent with our previous investigations by high-resolution fluorescence microscopy of fixed U2OS cells (25).

Stable U2OS lines expressing one GFP-tagged remodeler variant were used to measure the expression level of the endogenous remodelers. The concentrations of GFP-tagged remodelers were determined by FCS experiments (Table S1). Subsequently, quantitative Western blotting was used to measure the ratio of endogenous remodelers relative to the GFP-tagged ones (Fig. S2). The expression levels of Snf2H-GFP and GFP-Snf2L+13 were about twofold higher than those of the corresponding endogenous proteins, whereas endogenous Snf2L was not detectable in the U2OS cell line. From the combined FCS/Western blot analysis endogenous protein concentrations of 0.83 ± 0.13 μM (Snf2H), >0.15 ± 0.03 μM (hACF complex formed by Snf2H and Acf1), <0.05 μM (Snf2L), and 0.14 ± 0.04 μM (Snf2L+13) were determined.

The remodeling activity of the GFP-tagged proteins was evaluated in in vitro experiments (Fig. S3). As expected, both Snf2H-GFP and GFP-Snf2L were capable of translocating nucleosomes whereas Snf2L+13 lacked any activity. In comparison with freely mobile recombinant His-tagged Snf2H and Snf2L, affinity-purified GFP-tagged remodelers tethered to agarose beads showed a somewhat lower translocation activity (Fig. S3 *B* and *C*). Immobilizing His-tagged recombinant proteins reduced their activity to similar levels, indicating that the GFP tag did not impair the catalytic function.

Snf2H-GFP and GFP-Snf2L Are Recruited to Replication Foci and DNA Repair Sites. Because Snf2H and Acf1 have been shown to play a role in replication (23), we studied the localization of Snf2H-GFP, GFP-Snf2L, and inactive GFP-Snf2L+13 in the S phase of the cell cycle (Fig. 1). Both Snf2H-GFP and GFP-Snf2L were enriched at replication foci as detected by colocalization with PCNA-RFP. Moreover, 40–70% fractions of the remodelers were immobilized at these sites as determined from CP curves acquired at the replication foci. Notably, no difference between active Snf2L and inactive Snf2L+13 was apparent. Besides replication, Snf2H has been shown to be involved in the DNA damage response via the Snf2H-WSTF complex (26). To investigate this process DNA damage was locally induced by microirradiation with a UV laser. Subsequent recruitment of PCNA-RFP and Snf2H-GFP to the damage site was observed. Interestingly, GFP-Snf2L and GFP-Snf2L+13 also accumulated at the damage site, suggesting a potential function of Snf2L in the DNA damage response. In contrast, no accumulation was found for GFP alone (Fig. S4). Bleaching experiments demonstrated that Snf2H-GFP and GFP-Snf2L as well as GFP-Snf2L+13 were immobilized at the repair sites (Fig. 1). The accumulation of inactive Snf2L+13 at replication foci and repair sites demonstrates that the recruitment occurs independent of ATPase activity. In summary, Snf2H-GFP reproduced the localization behavior reported previously for endogenous Snf2H (23, 26). In addition, Snf2H-GFP with GFP at the C terminus and N-terminally tagged RFP-Snf2H showed no differences regarding intracellular localization or mobility (Fig. S5). Thus, with respect to the experiments conducted here no influence of the autofluorescent protein domain on the mobility and interactions of the remodeler was detected.

Multimeric Snf2H and Acf1 Associate into a Heterotetramer or Higher-Order Complex. Acf1 is one of the noncatalytic subunits that can associate with the Snf2H/ISWI motor protein in a complex termed ACF (27, 28). To probe multimerization of Snf2H and Acf1 in living U2OS cells, their complexes containing proteins labeled in two different colors were evaluated by fluorescence cross-correlation spectroscopy (21, 29, 30). The FCCS analysis of cells transfected with either Snf2H-GFP and RFP-Snf2H or Acf1-GFP and Acf1-RFP revealed a high cross-correlation signal, which was indicative of the formation of Snf2H and Acf1 homodimers or higher-order complexes (Fig. 2, Table 1). From the amplitudes of the auto- and cross-correlation functions, the fraction of the total amount of protein incorporated into these complexes was calculated to be at least 82 ± 8% for Snf2H and 94 ± 6% for Acf1. In addition, the interaction of Acf1-RFP and Snf2H-GFP was probed by transfecting Acf1-RFP into U2OS

cells stably expressing Snf2H-GFP. The normalized degree of cross-correlation was $r_x = 0.22 \pm 0.04$ (Fig. 2, Table 1), which shows that both proteins interact. The simplest model to explain the FCCS results is the association of Snf2H and Acf1 homodimers into a heterotetrameric ACF complex (larger complexes would also be compatible with the data). For an ACF heterotetramer the fraction of the total cellular Snf2H pool in this complex is >18 ± 4%. Considering the contribution of unlabeled endogenous protein would increase this value.

Snf2H-GFP, GFP-Snf2L, and Acf1-GFP Are Only Transiently Associated with Chromatin in G1/2 Phase. The dynamics of Snf2H, Snf2L, and Snf2L+13 in living U2OS cells during G1/2 and S phase were characterized by a combination of FRAP and FCS experiments (Fig. 3, Tables 2 and 3). For all proteins the FRAP recovery curves could be fitted well with a diffusion model, in which the contribution of transient binding is included into an effective diffusion coefficient (19). Recovery in the FRAP experiments during G1 phase was almost complete with immobile fractions of only 1–4% (Table 2). During S phase the immobile fraction increased as observed in FRAP and CP experiments (Table 2, Fig. 1). The FRAP value of ~10% was lower than that of 40–70% estimated from the CP analysis because the bleached area in the FRAP experiments contained both replication foci and regions of low PCNA density. From an analysis of the FRAP data according to a reaction–diffusion model the lower limit of the dissociation rate in G1/2 phase was determined to be $k_{off} > 14\ s^{-1}$ ($t_{res} = 70$ ms) for Snf2H-GFP and $k_{off} > 8\ s^{-1}$ ($t_{res} = 130$ ms) for GFP-Snf2L (*SI Materials and Methods*). An upper limit for k_{off} could not be determined reliably in the FRAP analysis because the average residence time in the chromatin-bound state was too short. This question was addressed by FCS experiments that have a much better time resolution and yield the diffusion time τ in the nucleus as a direct readout from the intensity fluctuations in the focal volume. In addition, the remodelers' mobility can be measured also in the cytosol by FCS where both Snf2H and Snf2L are freely mobile and present at nanomolar concentration with $D = 13\ \mu m^2 \cdot s^{-1}$ or τ = ~0.6 ms (Table 3). Corresponding values in the nucleus were

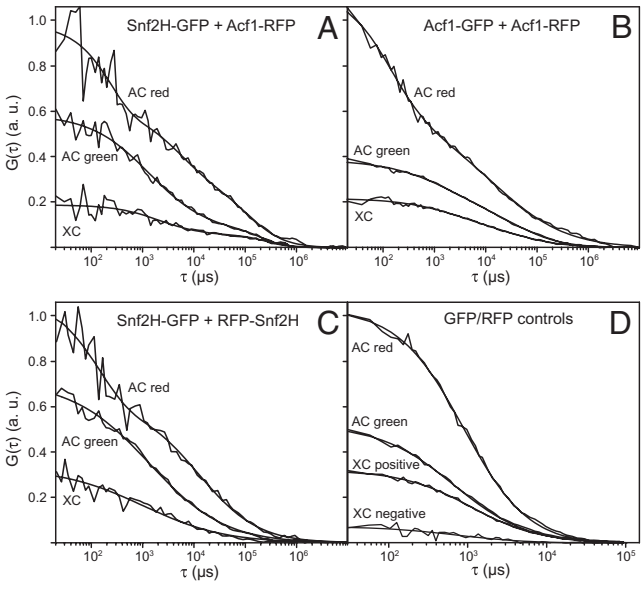

Fig. 2. Interactions of Snf2H and Acf1 probed by FCCS in the U2OS cell nucleus. The value of the ratio r_x (Table 1) calculated from the amplitudes of the cross-correlation and autocorrelation functions reveals the presence of complexes containing Snf2H-GFP and Acf1-RFP (*A*), Acf1-GFP and Acf1-RFP (*B*), and Snf2H-GFP and RFP-Snf2H (*C*). Auto- (AC) and cross-correlation (XC) functions of the two color channels are shown. (*D*) Control measurements in U2OS cells expressing a GFP–RFP fusion protein (XC positive) or GFP and RFP alone (XC negative).

Table 1. FCCS measurements of Snf2H and Acf1 interactis in the U2OS cell nucleus

Complex	D_{nuc} ($\mu m^2 \cdot s^{-1}$)	Ratio *G*	r_x	Complex, %
Snf2H-GFP·RFP-Snf2H	3.4 ± 0.6	0.35 ± 0.02	0.29 ± 0.02	>82 ± 8
Snf2H-GFP·Acf1-RFP	3.8 ± 1.5	0.29 ± 0.04	0.22 ± 0.04	>18 ± 4
Acf1-GFP·Acf1-RFP	2.9 ± 0.9	0.37 ± 0.03	0.32 ± 0.04	>94 ± 6

D_{nuc} is the diffusion coefficient of the complex determined from the cross-correlation analysis. The degree of cross-correlation r_x reflects the amount of complexes formed that carry both a GFP and an RFP label. For details on the FCCS analysis, see *SI Materials and Methods*.

2.0 ± 0.3 ms (Snf2H-GFP) and 1.2 ± 0.2 ms (GFP-Snf2L) for 70–80% of the molecules (Table 3). Furthermore, an additional slow population with $D_{slow} = 0.03$–$0.10\ \mu m^2 \cdot s^{-1}$ (τ = 100–600 ms) was present in the nucleus, which reflects chromatin translocations that manifest themselves as slow intensity fluctuations of bound fluorescently labeled proteins. This explanation is inferred from the value of the anomaly parameter α > 1, which is indicative of a confined diffusion behavior in the FCS analysis, and the observation that this contribution is a general feature of proteins that interact transiently with chromatin like heterochromatin protein 1 (19). This interpretation is corroborated by the absence of a corresponding mobility fraction in the FRAP experiments for Snf2H/Snf2L, where a <150 ms residence time and *D* values of 0.9 ± 0.1 and 1.0 ± 0.1 $\mu m^2 \cdot s^{-1}$ were measured (Table 2). Taken together, the FCS data clearly point to an average residence time of a few milliseconds for the vast majority of the remodeler fraction detectable by FCS (Table 3). Because immobilized molecules are typically bleached after 1 s, FCS provides no information about larger residence times. However, no remodelers bound on the timescale of seconds were found in the FRAP analysis and the remodeler fraction immobilized on the timescale of ≥1 min comprised only 1–4%. Thus, the short millisecond residence time applies for almost the whole remodeler pool during G1/2 phase.

To compare the mobility of the remodeler ATPases to the mobility of a noncatalytic complex subunit, U2OS cells were transiently transfected with Acf1-GFP. The FRAP and FCS analysis yielded effective diffusion coefficients and immobile fractions that were very similar to that of Snf2H-GFP (Fig. 3, Tables 2 and 3). These results indicate that there are no large differences between the dynamics and the interactions of Snf2H-GFP and Acf1-GFP.

Lack of ATPase Activity Leads to a Small Increase in Snf2H and Snf2L Mobility. To identify the contribution of the remodeling reaction to the mobility of Snf2H and Snf2L, the naturally occurring inactive splice variant Snf2L+13 was included in the analysis. In Snf2L+13 the exon 13 is spliced into the ATPase cassette of Snf2L, resulting in a noncatalytic protein. Because Snf2L+13 has been found in the same complexes as Snf2L, it could function as a dominant negative variant (24). Whereas the overall dynamic behavior of Snf2L+13 was similar to that of Snf2L and Snf2H, a small but significant increase in the mobility was apparent. The immobile fraction (1 ± 1%) was virtually absent for Snf2L+13 and a larger effective diffusion coefficient of 1.6 ± 0.1 $\mu m^2 \cdot s^{-1}$ was determined as compared with Snf2L with 3 ± 1% immobile protein and $D_{eff} = 1.0 \pm 0.1\ \mu m^2 \cdot s^{-1}$ (Fig. 3 *B* and *C*, Table 2). Similar results were obtained with transiently transfected HEK 293T cells (Fig. S6), which, in contrast to U2OS cells, express active Snf2L endogenously (31). Here, values of 2 ± 1% and 2.0 ± 0.4 $\mu m^2 \cdot s^{-1}$ (Snf2L) in comparison with 1 ± 1% and 2.7 ± 0.4 $\mu m^2 \cdot s^{-1}$ (Snf2L+13) for the effective diffusion coefficient and the immobile fraction were measured.

To further investigate differences between the active and the inactive state of Snf2L and Snf2H, U2OS cells were depleted of ATP by addition of sodium azide (Fig. 3 *A*–*D*). Because the remodeling reaction is ATP dependent, no remodeling is expected to occur under these conditions. The mobility of Snf2H-GFP and GFP-Snf2L was measured using FRAP and FCS as

CELL BIOLOGY

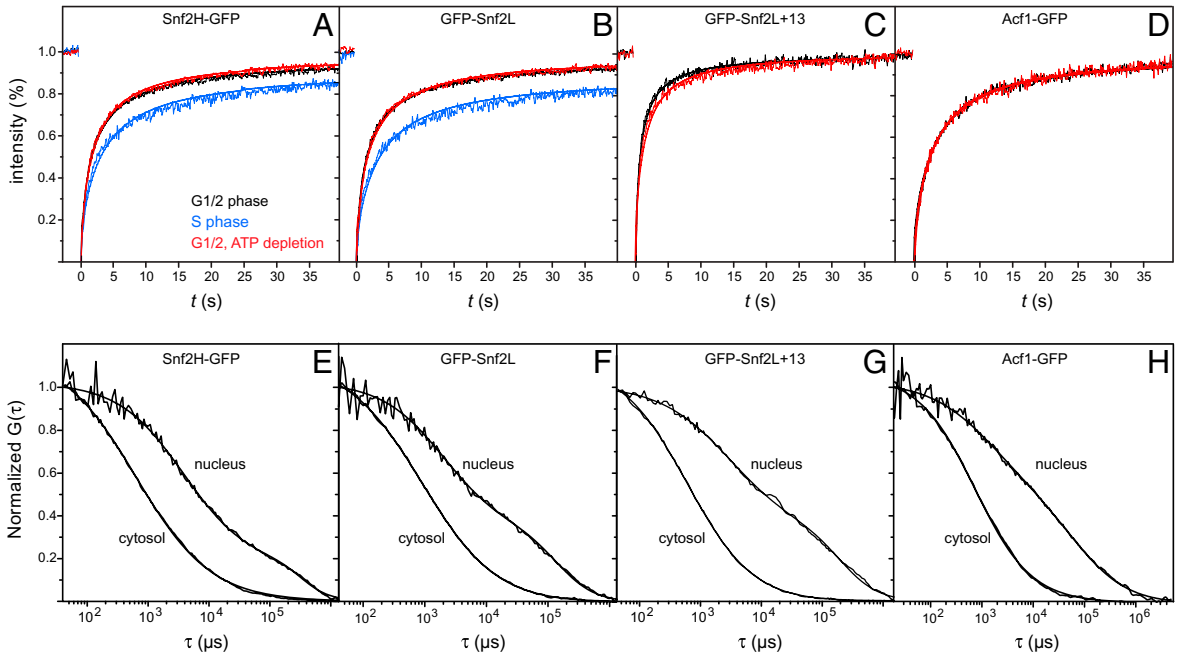

Fig. 3. Mobility of Snf2H-GFP, GFP-Snf2L, GFP-Snf2L+13, and Acf1-GFP. All proteins displayed a high mobility and only transient binding to chromatin during G1/2 phase (Tables 2 and 3) but an increased immobilized fraction was observed for Snf2H and Snf2L during S phase in U2OS cells. *A–D* show averaged FRAP curves, and *E–H* display single FCS experiments for the indicated proteins.

described above. The results were the same as those obtained in the comparison of Snf2L and Snf2L+13: A small reduction by 1–3% in the immobile fraction and a slight change of the effective diffusion coefficient toward a higher mobility in the ATP-depleted cells (Fig. 3 *A–D*, Table 2). Thus, the mobility differences between the active and the inactive (Snf2L+13, ATP-depleted Snf2H and Snf2L) case were significant but small. This result suggests that only a fraction of a few percent of the remodelers is actively involved in chromatin remodeling during G1/2 phase and displays an increased residence time in the chromatin-bound state.

Discussion

The translocation of nucleosomes by chromatin remodeling complexes was investigated previously in numerous in vitro studies (e.g., refs. 6–8, 13, 16, 17, 27, 28, 32, and references therein). However, details on their mode of operation in living cells are missing. Here, we analyzed the dynamics and interaction behavior of Snf2H, Snf2L, and Snf2L+13 as well as Acf1 in living cells with a multiscale approach that combined FRAP, CP, and FC(C)S experiments (18–21). In the case of FRAP, the shape of the recovery curve is used to extract dynamic parameters such as the diffusion coefficient and the kinetic rate constants. Furthermore, immobilized proteins are identified reliably from an incomplete recovery. CP has the advantage that immobilized protein fractions at loci as small as the optical resolution can be evaluated. FCS on the other hand yields information on the mobile protein fraction with high spatial and temporal resolution that is complementary to FRAP and CP.

Table 2. FRAP measurements in U2OS cells

Protein	D_{eff}, μm^2·s^{-1}		k_{off}, s^{-1}	Immobile, %	
	G1/2	S	G1/2	G1/2	S
Snf2H-GFP	0.9 ± 0.1	0.8 ± 0.1	>13.6 ± 2.3	4 ± 1	9 ± 2
Snf2H-GFP, no ATP	1.2 ± 0.1	0.8 ± 0.1	>12.3 ± 2.3	1 ± 0	9 ± 2
GFP-Snf2L	1.0 ± 0.1	0.6 ± 0.1	>8.3 ± 1.5	3 ± 1	9 ± 1
GFP-Snf2L, no ATP	1.2 ± 0.2	0.6 ± 0.2	>3.3 ± 0.4	2 ± 1	12 ± 3
GFP-Snf2L+13	1.6 ± 0.1	1.5 ± 0.7	>2.0 ± 0.4	1 ± 1	n.d.
GFP-Snf2L+13, no ATP	1.4 ± 0.2	n.d.	>7.7 ± 1.5	1 ± 0	n.d.
Acf1-GFP	0.9 ± 0.3	n.d.	>2.3 ± 0.8	3 ± 2	n.d.
Acf1-GFP, no ATP	0.7 ± 0.1	n.d.	>2.3 ± 0.5	0	n.d.

Measurements in S phase represent an average over several replication foci and regions of low PCNA density within the bleached region. n.d., not determined.

The FRAP, CP, and FCS experiments revealed that all proteins studied here were highly dynamic in the nucleus during G1/2 phase and bound only transiently to chromatin with upper limits for the residence times of <150 ms for Snf2H/L and <500 ms for Snf2L+13 and Acf1. These residence times are at the low end of values reported for other chromatin interacting proteins but similar to values for some transcription factors (18, 33). From a comparison of Snf2L and the inactive Snf2L+13 splice variant in conjunction with ATP depletion experiments we infer that only a small fraction of a few percent of a given ISWI type ATPase is involved in actively translocating nucleosomes during G1/2 phase. However, in replication foci during S phase or at DNA repair sites the fraction of tightly bound remodelers with residence times of at least several seconds is dramatically increased up to 40–70%. Because an increase of immobile Snf2L+13 was observed, too, binding to these sites occurs also independently of ATPase activity. This observation suggests a mechanism in which increasing the binding affinity of a given remodeler to its nucleosome substrate promotes nucleosome translocation as proposed previously on the basis of in vitro studies (6).

In the FCCS experiments the mutual homo- and heteromeric interactions of Snf2H and Acf1 were evaluated and demonstrated the simultaneous presence of Snf2H–Snf2H, Acf1–Acf1, and Snf2H–Acf1 interactions. Previous cryoelectron microscopy and FCCS in vitro work reported that dACF/hCHRAC is a heterotetramer composed of two Snf2H/ISWI and two Acf1 subunits (30, 34). Together with our FCCS results it is concluded that in the human cell nucleus hACF/hCHRAC heterotetramer complexes are formed via the equilibrium association of Snf2H and Acf1 dimers. The quantitative analysis of the FCCS data in terms of a homodimer–heterotetramer equilibrium results in a fraction of >18 ± 4% of the Snf2H pool being associated with Acf1. This

Table 3. FCS measurements in U2OS cells

Protein	D_{cyt}, $\mu m^2 \cdot s^{-1}$	D_{nuc}, $\mu m^2 \cdot s^{-1}$	f_{slow}, %	D_{slow}, $\mu m^2 \cdot s^{-1}$	α_{slow}	K^*_{bin}
Snf2H-GFP	13.0 ± 1.0	3.9 ± 0.4	22 ± 3	0.03 ± 0.01	2.1 ± 0.2	2.3 ± 0.7
GFP-Snf2L	13.3 ± 0.8	6.6 ± 0.4	29 ± 3	0.11 ± 0.01	1.5 ± 0.1	1.0 ± 0.3
GFP-Snf2L+13	13.0 ± 1.4	5.2 ± 0.4	25 ± 4	0.10 ± 0.01	1.3 ± 0.2	1.5 ± 0.5
Acf1-GFP	10.4 ± 0.5	3.5 ± 0.5	33 ± 5	0.07 ± 0.02	1.4 ± 0.3	2.0 ± 0.6

From the comparison of FCS measurements of diffusion coefficients in the cytosol (D_{cyt}) and in the nucleus (D_{nuc}) the pseudoequilibrium binding constant K^*_{bin} (K_{bin} multiplied with the binding site concentration) was determined. The larger value for Snf2H-GFP compared with GFP-Snf2L reflects either a higher binding affinity to chromatin or the presence of more binding sites than for GFP-Snf2L. The slow mobility fractions f_{slow} displayed a behavior indicative of a slowly, confinedly moving lattice that is characterized by $\alpha > 1$ in the FCS analysis.

value is the lower limit that does not consider the presence of unlabeled endogenous Snf2H and Acf1, which reduce the cross-correlation signal. Due to the presence of other Snf2H-containing complexes like NoRC or WSTF not the whole Snf2H pool is present in Acf1-containing complexes (8, 9, 26). Because the monomeric Snf2H fraction was determined to equal <18% (Table 1), these Snf2H-containing complexes are likely to comprise Snf2H multimers as well.

Using a combination of FCS and quantitative Western blots we were able to measure endogenous remodeler concentrations of 0.83 ± 0.13 μM (Snf2H), >0.15 ± 0.03 μM (hACF complex formed by Snf2H and Acf1), <0.05 μM (Snf2L), and 0.14 ± 0.04 μM (Snf2L+13) in the human U2OS cell line. To our knowledge these quantifications of remodeler concentrations in vertebrates/higher eukaryotes have not been described elsewhere. They point to a distinct pattern of different remodeling activities. Whereas the cell line-specific Snf2L protein is not detected in U2OS cells, its inactive splice variant was found at concentrations of 140 nM in the nucleus. In comparison, a specific type of active chromatin remodeler complex like hACF would be typically present at a concentration >100 nM. Extrapolating this value to the total concentration of all remodeling complexes and including complexes of the other ATPase families (Snf2, Mi-2, Chd1, Ino80, ERCC6, ALC1, CHD7, Swr1, RAD54, and Lsh), the total chromatin remodeler concentration in the human cell nucleus is estimated to be in the 10 μM range with a nucleosome concentration of 140 μM (35). Thus, the resulting remodeler/nucleosome ratio is similar to that of yeast with one remodeler per ~10 nucleosomes (36, 37). Because of their presence in high concentrations and the capability of complexes like ACF to bind >1 nucleosome, it has been proposed that ISWI chromatin remodelers might represent a stable structural component of chromatin (38). In the light of the high mobility of these complexes and the absence of a significant immobile fraction during G1/2 phase, such an architectural function during the whole cell cycle seems unlikely. Furthermore, several other conclusions on the mechanism by which chromatin remodeling complexes operate in living cells can be made (Fig. 4). The very short residence time in the chromatin-bound state during G1/2 phase reveals either that the remodeling reaction is too fast to be resolved or that only a very small remodeler fraction (<5%) is active at a given point of time. From in vitro data obtained with SWI/SNF remodelers, the velocity of chromatin remodeling can be estimated to equal ~13 $bp \cdot s^{-1}$ (39). Ensemble FRET studies with purified mononucleosomes and Snf2H resulted in even slower rates of 17 bp in a few seconds (40). Thus, the residence times measured here would be compatible with no or only a very small translocation of a few base pairs for the vast majority of the remodeling complexes. It is noted that such a small step size would be in contradiction to the experimentally observed remodeling behavior of ISWI remodelers, for which translocation steps of ~10–50 bp were reported (30). In addition, the ACF complex has been shown to be committed to its substrate for several minutes in vitro, further supporting the notion that the remodeling reaction does not occur within <150 ms (41, 42). Thus, we conclude that the 96–97% mobile remodeler fraction found here is not engaged in chromatin remodeling under "housekeeping" conditions in G1/2 phase. In contrast, the remodeling activity is high at replication foci during S phase or at DNA repair sites, and a large remodeler fraction immobilized for seconds to minutes was detected. Accordingly, active remodeling is associated with binding times at least on the second timescale. These binding times include contributions from the ATPase independent interactions with recruiting protein factors and the nucleosome translocation reaction itself. At these active sites, immobilized ISWI remodelers could also play a role for chromatin architecture.

In summary we propose a model, in which the chromatin remodelers continuously sample a large number of nucleosomes by transiently binding and dissociating without nucleosome translocation in G1/2 phase (Fig. 4*A*). In the default state the nucleosomes would be stably bound to their positions, as opposed to a "fluid" chromatin model, in which constant movements of the majority of nucleosomes would render most of the DNA accessible to interacting protein factors. Only upon introducing additional signals like, for example, core histone modifications at certain nucleosomes, the phosphorylation of the H2A.X variant as a DNA damage signal, or decoration with interacting proteins as during S phase or DNA repair (Fig. 4*B*), would these nucleosomes be marked "to be translocated" by making them high-affinity substrates. This view is supported by the

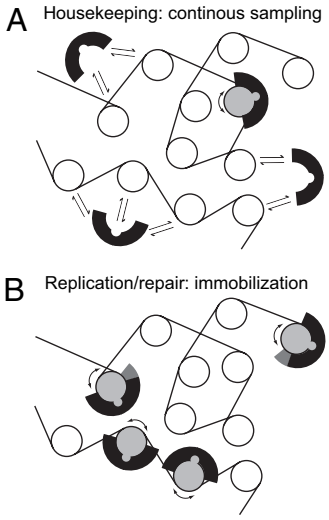

Fig. 4. ISWI chromatin remodeler interactions with chromatin. (*A*) During G1/2 phase chromatin remodelers bind only transiently to nucleosomes with residence times in the 10-ms regime and operate via a "continuous sampling mechanism." Most encounters are not productive and efficient nucleosome translocation requires additional signals that increase the binding affinity. These signals are present at only a small subset of nucleosomes during housekeeping conditions. (*B*) In S phase at replication foci or at sites of DNA repair remodeling "hotspots" exist. These hotspots are formed by increasing the binding of remodelers to the respective genomic loci to residence times in the range of seconds to minutes. Identification of a remodeling hotspot could be mediated by histone modifications, chromatin-associated proteins, or structural features of the chromatin environment.

results of several reports that demonstrate a connection between remodeling activity and histone modifications as reviewed in ref. 7. From the parameters measured here for the isolated Snf2H ATPase and its complex with Acf1 (endogenous protein concentration 0.15–0.83 μM, average residence time 75–430 ms) we estimate that nucleosomes are sampled at a rate of 0.1–3 min^{-1} by a specific ISWI-type complex. To probe 99% of all genomic nucleosomes, average sampling times of ~80 s (all Snf2H containing remodelers) and ~45 min (ACF) are calculated with the values from the FRAP analysis (*SI Materials and Methods* and Table S2). These results have to be regarded as upper limits because the average residence times in the order of 10 ms from the FCS analysis would decrease the corresponding sampling times to 11–64 s. Thus, after setting an appropriate signal a nucleosome can be translocated within tens of seconds or minutes to its new position. For this mechanism a relatively large concentration of remodelers is required to sample the ensemble of all nucleosomes in the genome at an acceptable speed. If the cell contained a 100-fold lower concentration of ISWI-type remodelers, i.e., a concentration of a few nanomolar, the sampling time would increase to hours. This would introduce a significant lag time for the readout of external signals on the timescale of cellular transitions. From this point of view a large pool of remodelers with only a small fraction of simultaneously active complexes seems mandatory to respond quickly to changes of the chromatin state. It is noted that these features of the continuous sampling mechanism are in excellent agreement with findings on cyclically occurring epigenetic processes that initiate and terminate remodeling of chromatin by SWI/SNF and NuRD complexes (33, 43, 44). In contrast, a large fraction of continuously active remodelers would constantly expose all parts of the DNA sequence to the surrounding nucleoplasm at much higher energy costs, because the remodelers' ATPase activity is stimulated by the bound nucleosome substrate (32). Thus, our findings point to a tight regulation of chromatin accessibility, realized by nucleosomes as switches that are continuously sampled by chromatin remodelers and triggered upon distinct signals.

Materials and Methods

Experiments were conducted with GFP and RFP constructs of human Snf2H, Snf2L, Snf2L+13, and Acf1 in human U2OS osteosarcoma, human embryonic kidney HEK293T, and mouse NIH 3T3 cell lines as described in *SI Materials and Methods*. For Snf2H-GFP, GFP-Snf2L, and GFP-Snf2L+13 stably transfected U2OS clones were derived. Other constructs were introduced via transient transfection. FRAP, CP, and F(C)CS experiments were conducted as described previously (19) and in *SI Materials and Methods*. At least 20 cells were measured for a given experimental condition. For FRAP the time evolution of the intensity integrated over the bleach spot was fitted to a diffusion model, to a binding model, or to a reaction–diffusion model that incorporates both diffusion and binding processes. In the CP experiments the decay of the fluorescence signal due to the dynamic equilibrium of photobleaching, diffusion, and chromatin dissociation/association of GFP-tagged proteins was used to measure the immobilized fraction with the resolution given by the confocal excitation volume. The FCS data were fitted to a one- or two-component anomalous diffusion model, which is characterized by a nonlinear time dependency of the mean squared particle displacement given by the anomaly parameter α.

ACKNOWLEDGMENTS. We thank Malte Wachsmuth for help and discussions, Patrick Varga-Weisz (Babraham Institute, Cambridge, UK) and David Picketts (Ottawa Health Research Institute, Ottawa, Canada) for plasmid vectors, and Hanswalter Zentgraf (Deutsches Krebsforschungszentrum, Heidelberg, Germany) for the Snf2L+13 antibody. This work was supported by Deutsche Forschungsgemeinschaft Grants Ri 1283/8-1 (to K.R.) and FOR1068 (to G.L.) and by the Baygene program of the Bavarian State Ministry of Sciences, Research, and the Arts (G.L.).

1. Radman-Livaja M, Rando OJ (2010) Nucleosome positioning: How is it established, and why does it matter? *Dev Biol* 339:258–266.
2. Jiang C, Pugh BF (2009) Nucleosome positioning and gene regulation: Advances through genomics. *Nat Rev Genet* 10:161–172.
3. Segal E, Widom J (2009) From DNA sequence to transcriptional behaviour: A quantitative approach. *Nat Rev Genet* 10:443–456.
4. Henikoff S (2008) Nucleosome destabilization in the epigenetic regulation of gene expression. *Nat Rev Genet* 9:15–26.
5. Flaus A, Martin DM, Barton GJ, Owen-Hughes T (2006) Identification of multiple distinct Snf2 subfamilies with conserved structural motifs. *Nucleic Acids Res* 34:2887–2905.
6. Rippe K, et al. (2007) DNA sequence- and conformation-directed positioning of nucleosomes by chromatin-remodeling complexes. *Proc Natl Acad Sci USA* 104:15635–15640.
7. Gangaraju VK, Bartholomew B (2007) Mechanisms of ATP dependent chromatin remodeling. *Mutat Res* 618:3–17.
8. He X, Fan HY, Garlick JD, Kingston RE (2008) Diverse regulation of SNF2h chromatin remodeling by noncatalytic subunits. *Biochemistry* 47:7025–7033.
9. Corona DF, Tamkun JW (2004) Multiple roles for ISWI in transcription, chromosome organization and DNA replication. *Biochim Biophys Acta* 1677:113–119.
10. Bork P, Koonin EV (1993) An expanding family of helicases within the 'DEAD/H' superfamily. *Nucleic Acids Res* 21:751–752.
11. Eisen JA, Sweder KS, Hanawalt PC (1995) Evolution of the SNF2 family of proteins: Subfamilies with distinct sequences and functions. *Nucleic Acids Res* 23:2715–2723.
12. Boyer LA, Latek RR, Peterson CL (2004) The SANT domain: A unique histone-tail-binding module? *Nat Rev Mol Cell Biol* 5:158–163.
13. Grüne T, et al. (2003) Crystal structure and functional analysis of a nucleosome recognition module of the remodeling factor ISWI. *Mol Cell* 12:449–460.
14. Eberharter A, Becker PB (2004) ATP-dependent nucleosome remodelling: Factors and functions. *J Cell Sci* 117:3707–3711.
15. Banting GS, et al. (2005) CECR2, a protein involved in neurulation, forms a novel chromatin remodeling complex with SNF2L. *Hum Mol Genet* 14:513–524.
16. Längst G, Becker PB (2001) Nucleosome mobilization and positioning by ISWI-containing chromatin-remodeling factors. *J Cell Sci* 114:2561–2568.
17. Narlikar GJ, Fan HY, Kingston RE (2002) Cooperation between complexes that regulate chromatin structure and transcription. *Cell* 108:475–487.
18. Wachsmuth M, Caudron-Herger M, Rippe K (2008) Genome organization: Balancing stability and plasticity. *Biochim Biophys Acta* 1783:2061–2079.
19. Müller KP, et al. (2009) Multiscale analysis of dynamics and interactions of heterochromatin protein 1 by fluorescence fluctuation microscopy. *Biophys J* 97:2876–2885.
20. Michelman-Ribeiro A, et al. (2009) Direct measurement of association and dissociation rates of DNA binding in live cells by fluorescence correlation spectroscopy. *Biophys J* 97:337–346.
21. Haustein E, Schwille P (2007) Fluorescence correlation spectroscopy: Novel variations of an established technique. *Annu Rev Biophys Biomol Struct* 36:151–169.
22. Leonhardt H, et al. (2000) Dynamics of DNA replication factories in living cells. *J Cell Biol* 149:271–280.
23. Collins N, et al. (2002) An ACF1-ISWI chromatin-remodeling complex is required for DNA replication through heterochromatin. *Nat Genet* 32:627–632.
24. Barak O, Lazzaro MA, Cooch NS, Picketts DJ, Shiekhattar R (2004) A tissue-specific, naturally occurring human SNF2L variant inactivates chromatin remodeling. *J Biol Chem* 279:45130–45138.
25. Gunkel M, et al. (2009) Dual color localization microscopy of cellular nanostructures. *Biotechnol J* 4:927–938.
26. Xiao A, et al. (2009) WSTF regulates the H2A.X DNA damage response via a novel tyrosine kinase activity. *Nature* 457:57–62.
27. Ito T, et al. (1999) ACF consists of two subunits, Acf1 and ISWI, that function cooperatively in the ATP-dependent catalysis of chromatin assembly. *Genes Dev* 13:1529–1539.
28. Poot RA, et al. (2000) HuCHRAC, a human ISWI chromatin remodelling complex contains hACF1 and two novel histone-fold proteins. *EMBO J* 19:3377–3387.
29. Rippe K (2000) Simultaneous binding of two DNA duplexes to the NtrC-enhancer complex studied by two-color fluorescence cross-correlation spectroscopy. *Biochemistry* 39:2131–2139.
30. Strohner R, et al. (2005) A 'loop recapture' mechanism for ACF-dependent nucleosome remodeling. *Nat Struct Mol Biol* 12:683–690.
31. Barak O, et al. (2003) Isolation of human NURF: A regulator of Engrailed gene expression. *EMBO J* 22:6089–6100.
32. Boyer LA, et al. (2000) Functional delineation of three groups of the ATP-dependent family of chromatin remodeling enzymes. *J Biol Chem* 275:18864–18870.
33. Hager GL, McNally JG, Misteli T (2009) Transcription dynamics. *Mol Cell* 35:741–753.
34. Hu M, et al. (2008) Three-dimensional structure of human chromatin accessibility complex hCHRAC by electron microscopy. *J Struct Biol* 164:263–269.
35. Weidemann T, et al. (2003) Counting nucleosomes in living cells with a combination of fluorescence correlation spectroscopy and confocal imaging. *J Mol Biol* 334:229–240.
36. Ghaemmaghami S, et al. (2003) Global analysis of protein expression in yeast. *Nature* 425:737–741.
37. Huh WK, et al. (2003) Global analysis of protein localization in budding yeast. *Nature* 425:686–691.
38. Varga-Weisz PD, Becker PB (2006) Regulation of higher-order chromatin structures by nucleosome-remodelling factors. *Curr Opin Genet Dev* 16:151–156.
39. Zhang Y, et al. (2006) DNA translocation and loop formation mechanism of chromatin remodeling by SWI/SNF and RSC. *Mol Cell* 24:559–568.
40. Yang JG, Narlikar GJ (2007) FRET-based methods to study ATP-dependent changes in chromatin structure. *Methods* 41:291–295.
41. Fyodorov DV, Kadonaga JT (2002) Dynamics of ATP-dependent chromatin assembly by ACF. *Nature* 418:897–900.
42. Gangaraju VK, Prasad P, Srour A, Kagalwala MN, Bartholomew B (2009) Conformational changes associated with template commitment in ATP-dependent chromatin remodeling by ISW2. *Mol Cell* 35:58–69.
43. Métivier R, et al. (2003) Estrogen receptor-alpha directs ordered, cyclical, and combinatorial recruitment of cofactors on a natural target promoter. *Cell* 115:751–763.
44. George AA, Schiltz RL, Hager GL (2009) Dynamic access of the glucocorticoid receptor to response elements in chromatin. *Int J Biochem Cell Biol* 41:214–224.

Supporting Information

Erdel et al. 10.1073/pnas.1003438107

SI Materials and Methods

Plasmid Vectors and Cell Lines. The plasmids pEGFP-N3-Snf2H and pEGFP-N1-Acf1 were kindly provided by Patrick Varga-Weisz and contain the full coding sequence of human Snf2H or Acf1 fused to GFP at the C terminus, referred to as Snf2H-GFP and Acf1-GFP (1). The coding sequences of human Snf2L and Snf2L+13 generously provided by David Picketts (2, 3) were cloned into pEGFP-C1 (Clontech) to construct the GFP-Snf2L and GFP-Snf2L+13 vectors. The red fluorescent derivatives RFP-Snf2H and Acf1-RFP were generated by cloning the coding sequence into pTagRFP-N1 or pTagRFP-C1 (Evrogen). The mRFP1-labeled histone H2A (H2A-RFP) and proliferating cell nuclear antigen (PCNA-RFP) have been described previously (4, 5). For FCCS analyses, an mRFP1-GFP fusion construct was used for comparison, which was kindly provided by Malte Wachsmuth (European Molecular Biology Laboratory, Heidelberg, Germany).

Cell Culture, Immunoprecipitation, and Western Blotting. Cells of the human U2OS osteosarcoma cell line (HTB-96) were cultured in DMEM/10% FCS, NIH 3T3 cells were cultured in DMEM High Glucose/10% FCS. For Snf2H-GFP, GFP-Snf2L and GFP-Snf2L+13 stably transfected U2OS clones were derived. Other constructs were introduced via transient transfection. For FRAP and FCS experiments as well as live imaging cells were grown in LabTek chambers (Nunc). ATP depletion was done as described previously by adding sodium azide to a final concentration of 10 mM (6). Measurements were performed after 20–30 min incubation. For immunostaining, cells were cultured in 12-well plates, and fixation was carried out using 4% paraformaldehyde/PBS for 7 min. For the production of cell lysates, U2OS cells were grown to confluence, harvested, and incubated on ice for 30 min in lysis buffer [10 mM Tris/Cl (pH 7.5), 150 mM NaCl, 0.5 mM EDTA, 0.1% Nonidet P-40] supplemented with a "complete" protease inhibitor mixture (Roche). Subsequently, membrane fragments were removed by centrifugation. For immunoprecipitation of GFP-tagged proteins, equilibrated Sepharose beads coupled to GFP-binding protein (GBP) (Chromotek) were added to the cell lysate and incubated for 1–2 h at 4 °C. Captured proteins were eluted by boiling in SDS-containing elution buffer and loaded onto a polyacrylamide gel. Proteins were transferred on nitrocellulose membranes (Whatman), using a wet-blot system (BioRad). Membranes were incubated with primary antibodies directed against Snf2H (no. 07-624; Upstate), Snf2L (ab37003; Abcam), or Snf2L+13 (Hanswalter Zentgraf, Deutsches Krebsforschungszentrum, Heidelberg, Germany) and secondary antibodies coupled to horseradish peroxidase. For detection, membranes were incubated with ECL solution and imaged with a CCD system (Intas). Alternatively, secondary antibodies coupled to DyLight 680 or DyLight 800 dyes were used and the signal was detected with a LI-COR Odyssey system (LI-COR Biosciences). Both methods yielded identical results.

In Vitro Activity Assay of GFP-Tagged ATPases Snf2H and Snf2L. The activity of the GFP-tagged remodelers was tested in an in vitro assay. First, Snf2H-GFP, GFP-Snf2L, and the splice variant GFP-Snf2L+13 were purified from transiently transfected HEK293T cells, using the GFP-Trap system (Chromotek) according to the manufacturer's protocol. Second, the matrix-bound proteins were incubated with nucleosomes reconstituted on a Cy5-labeled DNA fragment containing the 601 nucleosome positioning sequence and ATP. Nucleosome remodeling reactions were performed as described (7). For one reaction, 0.02 pmol nucleosomes and 0.3 ± 0.1 pmol of the His-tagged remodelers in solution (Fig. S3*B* and His-Snf2L in Fig. S3*D*) or 0.9 ± 0.3 pmol of the remodelers bound to agarose beads (Fig. S3*C* and GFP-Snf2L/L+13 in Fig. S3*D*) were used. Nucleosome positions were resolved on 6% native polyacrylamide gels containing 0.5× TBE and scanned with the Fuji FLA-5000 fluorescence system.

Continuous Photobleaching and UV Microirradiation. Continuous photobleaching experiments were conducted with a Zeiss LSM 710 ConfoCor3. Medium laser intensities (~10% of the Lasos Argon laser operated in standby mode) were used for bleaching. CP data were analyzed as described previously (8, 9). All curves measured here could be successfully fitted with a model incorporating an immobile fraction and a mobile pool:

$$I(t) = f_{\text{immo}}\left(1 + \frac{\alpha t}{2} + \frac{\alpha^2 t^2}{6}\right)^{-1} + (1 - f_{\text{immo}})\exp(-\beta t).$$

α and β denote the bleach rates for the immobile and the mobile pool, respectively; f_{immo} is the immobile fraction. This expression corresponds to the equation derived previously with $k_{\text{off}} = 0$ (8). For UV microirradiation a region of interest was irradiated with the 405-nm laser line at maximum power for ~10 s to introduce DNA damage.

Fluorescence Recovery After Photobleaching. FRAP experiments were carried out on a Leica SP5 microscope. Images were acquired with 128 × 128 pixels in size and a scanning speed of 1,400 Hz. Typically 30 images were acquired before the bleach, 2 images were used for bleaching, and up to 500 images were acquired after the bleach. The shape of the bleached region of interest (ROI) was chosen to be circular because in this case an analytical solution for the Laplace transform of the recovery curve can be found. The diameter of the ROI was between 3 and 5 μm. The location of the ROI was selected in a way that between the cell boundary and the ROI sufficient space remained: This positioning is important to meet the assumption that the recovery does not depend on the local geometry and occurs in an isotropic fashion. Typically, 20–30 cells were analyzed for a given experimental condition. For the average values of the effective diffusion coefficient, each FRAP curve was fitted, the normalized diffusion times (i.e., the inverse diffusion coefficients) from each individual fit were averaged, and the resulting diffusion coefficient was calculated on the basis of the averaged diffusion time.

FRAP analysis was conducted with the software FREDIS (9). Recovery curves were fitted to a diffusion model, a reaction model, and a reaction–diffusion model (10). The diffusion model is suitable if no binding sites or binding sites with very high dissociation rates are present (effective diffusion). The reaction model describes the recovery if a binding site with a small dissociation rate is present, and the reaction–diffusion model describes the recovery in the presence of immobile binding sites with dissociation rate constant k_{off}. The expressions for the different models are as follows:

$$\text{diffusion model}: frap(t) = e^{-\frac{\tau_D}{2t}}\left[I_0\left(\frac{\tau_D}{2t}\right) + I_1\left(\frac{\tau_D}{2t}\right)\right]$$

$$\text{reaction model}: frap(t) = 1 - C_{\text{eq}}\, e^{-k_{\text{off}} t}$$

reaction-diffusion model:

$$\overline{frap}(p) = \frac{1}{p} - \frac{F_{eq}}{p}\left(1 - 2K_1(qw)I_1(qw)\right)\left(1 + \frac{k^*_{on}}{p + k_{off}}\right) - \frac{C_{eq}}{p + k_{off}}.$$

C_{eq} and F_{eq} denote the bound and the free fraction, k^*_{on} and k_{off} denote the pseudoassociation rate and the dissociation rate, τ_D is the diffusion time, I_0 and I_1 are modified Bessel functions, w is the bleach radius, and $q^2 = p/D_f\left(1 + k^*_{on}/(p + k_{off})\right)$. Because there is no analytical solution in the case of the reaction–diffusion model, the solution for the inverse Laplace transform is given (p is the complex Laplace variable).

The different fits were compared with each other on the basis of the F ratio, which depends on the fit qualities (χ^2 values) and the number of fit parameters in each model. A model with more fit parameters is expected to fit better than a simpler model. Accordingly, the number of fit parameters has to be accounted for when comparing different models. All proteins studied in this work exhibited effective diffusion behavior because their recoveries could be fitted with the diffusion-dominant model, but the diffusion coefficients obtained in the nucleus were significantly smaller than the (free) diffusion coefficients measured in the cytosol. Because viscosity and crowding effects are similar in the nucleus and the cytosol (as revealed by the analysis of GFP in the nucleus and the cytosol) (11), the reduced diffusion coefficient can be explained by chromatin interaction. Using the expression for the reaction–diffusion model (which fitted the data equally well compared with the diffusion-dominant model), the 95% confidence interval for k_{off} was determined. These confidence intervals became very large in the case of effective diffusion because the recovery essentially depends on the ratio of the rate constants k^*_{on}/k_{off}. The confidence intervals ranged from some lower limit for k_{off} to infinity; i.e., for k_{off} values above this lower limit good fits were obtained by adjusting the other fit parameters accordingly. In this manner only a lower limit for the dissociation rate k_{off} could be determined from the FRAP analysis.

Fluorescence Correlation Spectroscopy. For FCS experiments, a Leica TCS SP2 AOBS FCS2 system or a Zeiss LSM 710 ConfoCor3 was used. Typical acquisition times were in the range of 60 s. Before every measurement, a calibration with Alexa 488 C5 maleimide (Invitrogen) was performed. Similar laser intensities were used for the measurement of the samples and the controls. Data acquisition was with the programs Vista 3.6.22 (ISS) for the Leica SP2 and ZEN (Zeiss) for the Zeiss LSM 710. FCS data were analyzed as described previously (9). The autocorrelation function was calculated, and in the case of bleaching a moving average trend correction was applied. The autocorrelation function was fitted with the formula for anomalous diffusion (with one or two components):

$$G(\tau) = \frac{1}{N}\left(f_1 * \left(1 + \left(\frac{\tau}{\tau_{D,1}}\right)^{\alpha_1}\right)^{-1}\left(1 + \frac{1}{\kappa^2}\left(\frac{\tau}{\tau_{D,1}}\right)^{\alpha_1}\right)^{-\frac{1}{2}} + (1 - f_1)\left(1 + \left(\frac{\tau}{\tau_{D,2}}\right)^{\alpha_2}\right)^{-1}\left(1 + \frac{1}{\kappa^2}\left(\frac{\tau}{\tau_{D,2}}\right)^{\alpha_2}\right)^{-\frac{1}{2}}\right).$$

Here, N denotes the particle number, f_1 the size of the first component, $\tau_{D,1}$ and $\tau_{D,2}$ are the diffusion times for the first and the second component, κ is the structure parameter of the microscope's focal volume, and α_1 and α_2 are the anomaly parameters for the first and the second component. Typical fits had R^2 values >0.95 and uncorrelated residues. At least 20 measurements were performed for each protein in the nucleus and in the cytosol.

For FCCS, the cross-correlation function between the GFP and the RFP signals was calculated and fitted with the same formula given above. The degree of cross-correlation *ratio G* was calculated according to

$$ratio\ G = \frac{G_x(0)}{\sqrt{G_{GFP}(0) \cdot G_{RFP}(0)}}.$$

Here, $G_x(0)$ denotes the amplitude of the cross-correlation function and $G_{GFP}(0)$ and $G_{RFP}(0)$ denote the amplitudes of the autocorrelation function in the green and the red channel at lag time $\tau = 0$, respectively. The degree of cross-correlation *ratio* G_{sample} was normalized using the values for the negative (*ratio* G_{neg}) and positive (*ratio* G_{pos}) controls as described previously (12–14):

$$r_x = \frac{ratio\ G_{sample} - ratio\ G_{neg}}{ratio\ G_{pos} - ratio\ G_{neg}}.$$

TetraSpeck 0.1-μm fluorescent microspheres (Invitrogen) were used as a positive control, and U2OS cells cotransfected with GFP and RFP were used as a negative control. It is noted that the formula given above is applicable only if the concentrations of the green- and the red-labeled proteins are similar to each other in the negative control as well as in the sample, which was ensured in the experiments presented here. From r_x the fraction θ of protein in the complex was calculated, which depends on the complex composition and the ratios between labeled (GFP- or RFP-tagged) and unlabeled (endogenous) protein. For heterodimers AB of two proteins A and B labeled with different fluorophores, e.g., A-GFP and B-RFP, the following relation holds:

$$r_{x,AB} = \sqrt{\lambda_A \lambda_B \theta_A \theta_B}.$$

Here, λ_A and λ_B are the labeling degrees of proteins A and B, i.e., the amount of labeled protein divided by the total amount of protein of one type, and θ_A and θ_B are the fractions of monomers A and B in the complex. For the A_2B_2 heterotetramer, the degree of protein in the complex is derived from the normalized cross-correlation signal

$$r_{x,A2B2} = \sqrt{\frac{4\lambda_A \lambda_B \theta_A \theta_B}{(1 + \theta_A \lambda_A)(1 + \theta_B \lambda_B)}} = \frac{2}{\sqrt{(1 + \theta_A \lambda_A)(1 + \theta_B \lambda_B)}} r_{x,AB}.$$

The maximum value of r_x is higher for the A_2B_2 than for the AB complex because in the heterotetramer the probability to have complexes that carry only red or only green labels is lower.

To study self-association a protein can be labeled with two different fluorophores, e.g., A-GFP and A-RFP. For a homodimer A_2 (or a heterotetramer A_2B_2, which is equivalent if B is not labeled), the degree of cross-correlation is given by

$$r_{x,A2} = \sqrt{\frac{\lambda_A \lambda_B \theta_A \theta_B}{(1 + \theta_A \lambda_A)(1 + \theta_B \lambda_B)}}.$$

Here, the labeling degrees λ_A and λ_B equal the amount of protein A labeled with one fluorophore divided by the total amount of A. Thus, in contrast to the case of heteromultimerization, the sum of the two labeling degrees $\lambda_A + \lambda_B$ cannot be >1. In the absence of unlabeled protein and a 1:1 ratio of both fluorophores, $\lambda_A = \lambda_B = 0.5$.

Calculation of Remodeler–Nucleosome Sampling Rates. On the basis of the parameters measured, the sampling rate for remodeler–

nucleosome contacts was determined. The time that a remodeler spends in the chromatin-bound state is $\tau_{bound} = 1/k_{off}$, and the time in the freely diffusible state is $\tau_{free} = 1/(k_{on}c_N)$, with k_{off} and k_{on} being the dissociation/association rates and c_N the nucleosome concentration. Because the concentration of nucleosomes as potential binding sites is much larger than the remodeler concentration, the binding process can be described by a pseudo-first-order reaction. To probe one nucleosome, the remodeler requires $\tau_{search} = \tau_{bound} + \tau_{free}$. For c_R being the remodeler concentration, c_R nucleosomes are probed within τ_{search}. Thus, the minimum sampling time is $\tau_{sample,min} = (c_N/c_R)\tau_{search} = (c_N/c_R)\cdot(\tau_{bound} + \tau_{free})$ if every nucleosome is probed exactly once. This expression can be reformulated in terms of the pseudoaffinity $K^*_{bin} = (k_{on}\, c_N)/k_{off}$:

$$\tau_{\text{sample, min}} = \frac{c_N}{c_R k_{off}}\left(1 + \frac{1}{K^*_{bin}}\right).$$

Because the concentration of nucleosomes in the cell nucleus has been measured to be $c_N = 140$ μM (15), the sampling time can be calculated using the values for the dissociation rate (estimated from the FRAP analyses, Table 2), the pseudoaffinity (determined by FCS measurement, Table 3), and the endogenous remodeler concentration (determined by FCS and Western blotting, Table S1). Considering that not every nucleosome is probed exactly once, the actual sampling time turns out to be larger than the minimum sampling time $\tau_{sample,min}$. The remodelers' mode of action can be regarded as sequential cycles of searching and binding, each cycle requiring the time τ_{search}. The fraction of probed remodelers in each cycle is c_R/c_N. After the first cycle, $p_1 = c_R/c_N$ nucleosomes are probed, and after n cycles, the number of probed nucleosomes can be expressed according to the binomial distribution:

$$p_n = \sum_{k=1}^{n} \frac{n!}{k!(n-k)!}\left(\frac{c_R}{c_N}\right)^k \left(1-\frac{c_R}{c_N}\right)^{n-k} = 1-\left(1-\frac{c_R}{c_N}\right)^n.$$

By inverting this relation, the number of cycles n required for a given coverage p_n equals

$$n = \frac{\ln(1-p_n)}{\ln\left(1-\frac{c_R}{c_N}\right)}.$$

The corresponding sampling time $\tau_{sample,\,coverage}$ is the product of the required cycles n and the search time τ_{search} calculated above:

$$\tau_{\text{sample, coverage}} = \frac{n}{k_{off}}\left(1 + \frac{1}{K^*_{bin}}\right) = \frac{\ln(1-p_n)}{\ln\left(1-\frac{c_R}{c_N}\right)k_{off}}\left(1 + \frac{1}{K^*_{bin}}\right).$$

The resulting sampling times for 99% nucleosome coverage are summarized in Table S2. The minimum sampling time $\tau_{sample,\,min}$ corresponds to 63% nucleosome coverage.

1. Collins N, et al. (2002) An ACF1-ISWI chromatin-remodeling complex is required for DNA replication through heterochromatin. *Nat Genet* 32:627–632.
2. Barak O, Lazzaro MA, Cooch NS, Picketts DJ, Shiekhattar R (2004) A tissue-specific, naturally occurring human SNF2L variant inactivates chromatin remodeling. *J Biol Chem* 279:45130–45138.
3. Barak O, et al. (2003) Isolation of human NURF: A regulator of Engrailed gene expression. *EMBO J* 22:6089–6100.
4. Jegou T, et al. (2009) Dynamics of telomeres and promyelocytic leukemia nuclear bodies in a telomerase-negative human cell line. *Mol Biol Cell* 20:2070–2082.
5. Gunkel M, et al. (2009) Dual color localization microscopy of cellular nanostructures. *Biotechnol J* 4:927–938.
6. Görisch SM, et al. (2004) Nuclear body movement is determined by chromatin accessibility and dynamics. *Proc Natl Acad Sci USA* 101:13221–13226.
7. Längst G, Bonte EJ, Corona DF, Becker PB (1999) Nucleosome movement by CHRAC and ISWI without disruption or trans-displacement of the histone octamer. *Cell* 97: 843–852.
8. Wachsmuth M, et al. (2003) Analyzing intracellular binding and diffusion with continuous fluorescence photobleaching. *Biophys J* 84:3353–3363.
9. Müller KP, et al. (2009) Multiscale analysis of dynamics and interactions of heterochromatin protein 1 by fluorescence fluctuation microscopy. *Biophys J* 97:2876–2885.
10. Sprague BL, Pego RL, Stavreva DA, McNally JG (2004) Analysis of binding reactions by fluorescence recovery after photobleaching. *Biophys J* 86:3473–3495.
11. Pack C, Saito K, Tamura M, Kinjo M (2006) Microenvironment and effect of energy depletion in the nucleus analyzed by mobility of multiple oligomeric EGFPs. *Biophys J* 91:3921–3936.
12. Rippe K (2000) Simultaneous binding of two DNA duplexes to the NtrC-enhancer complex studied by two-color fluorescence cross-correlation spectroscopy. *Biochemistry* 39: 2131–2139.
13. Strohner R, et al. (2005) A 'loop recapture' mechanism for ACF-dependent nucleosome remodeling. *Nat Struct Mol Biol* 12:683–690.
14. Weidemann T, Wachsmuth M, Tewes M, Rippe K, Langowski J (2002) Analysis of ligand binding by two-colour fluorescence cross-correlation spectroscopy. *Single Mol* 3:49–61.
15. Weidemann T, et al. (2003) Counting nucleosomes in living cells with a combination of fluorescence correlation spectroscopy and confocal imaging. *J Mol Biol* 334: 229–240.

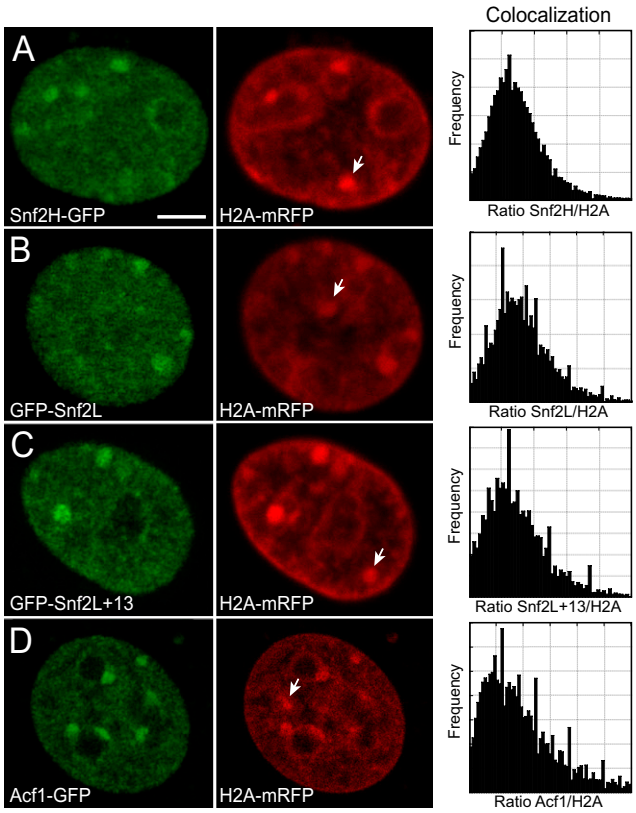

Fig. S1. Snf2H, Snf2L, Snf2L+13, and Acf1 bind chromatin in 3T3 cells. (*A–D*) Snf2H-GFP, GFP-Snf2L, GFP-Snf2L+13, and Acf1-GFP were transiently transfected into NIH 3T3 cells stably expressing H2A-RFP. In all cases, colocalization of the GFP-tagged proteins with H2A-RFP was observed, reflecting their ability to bind chromatin. To determine if the proteins were enriched in the dense heterochromatin foci of 3T3 cells, the ratio between the GFP and the RFP signal was calculated for each pixel and plotted into a histogram. Because the ratio was similar throughout the cell, there was no specific enrichment in heterochromatin. However, loci with decreased remodeler density were present (white arrows).

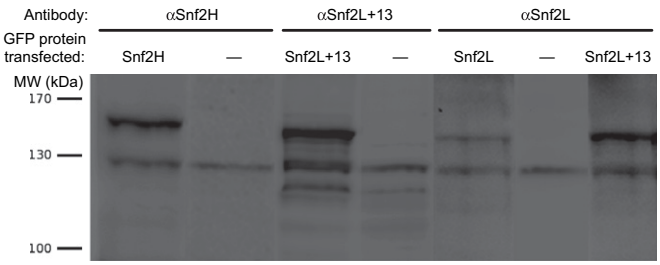

Fig. S2. Expression level of endogenous remodelers. Quantitative Western blotting was used to determine the relative expression levels of the GFP-tagged remodelers in the stable U2OS cell lines. (Lanes 1 and 2) U2OS/Snf2H-GFP and U2OS-WT incubated with anti-Snf2H; (lanes 3 and 4) U2OS/GFP-Snf2L+13 and U2OS-WT incubated with anti-Snf2L+13; (lanes 5 and 6) U2OS/GFP-Snf2L and U2OS-WT incubated with anti-Snf2L; (lane 7) U2OS/GFP-Snf2L+13 incubated with anti-Snf2L. Ratios between GFP-tagged and endogenous proteins of 2.4 ± 0.3 (lane 1), 1.8 ± 0.1 (lane 3), 0.8 ± 0.1 (lane 5), and 1.8 ± 0.1 (lane 7) were determined. The predicted molecular weight for Snf2H and Snf2L is 125 kDa, and the predicted molecular weight for GFP-tagged Snf2H/Snf2L is 152 kDa.

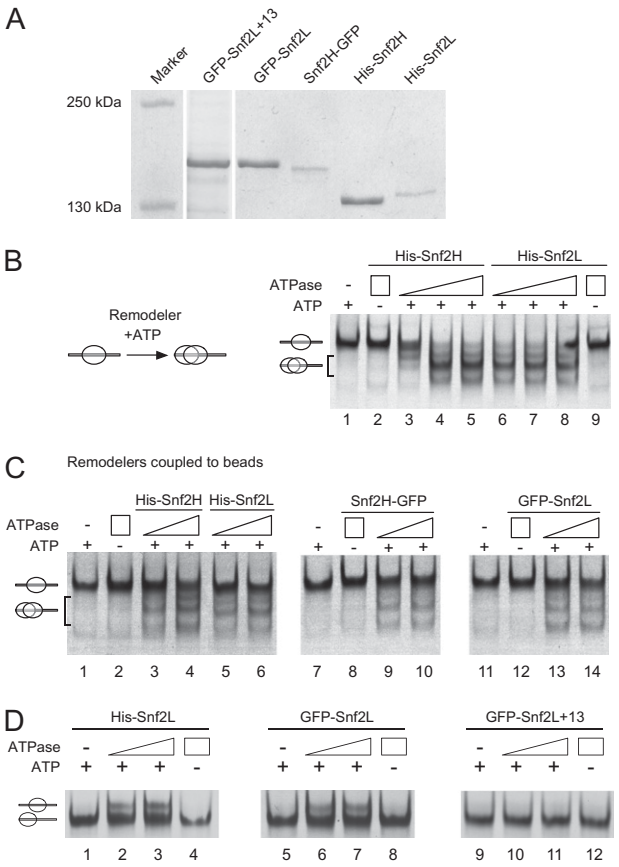

Fig. S3. Snf2H-GFP and GFP-Snf2L are catalytically active chromatin remodelers. (*A*) Remodeling ATPases were purified from baculovirus-infected Sf9 cells (His-Snf2H and His-Snf2L) or purified from transiently transfected HEK293T cells (Snf2H-GFP, GFP-Snf2L, and GFP-Snf2L+13). Purified proteins were analyzed by 6% SDS/PAGE and Coomassie blue staining. (*B*) Snf2H and Snf2L efficiently move nucleosomes from the center to more lateral positions of the nucleosomal 601 DNA containing 40 bp of DNA linkers on each side of the 601 sequence. Nucleosomes were incubated with increasing concentrations of Snf2H and Snf2L, in the presence (lanes 3–8) or in the absence of ATP (lanes 2 and 9). Nucleosome positions are indicated. (*C*) Bead-bound Snf2H and Snf2L exhibit reduced remodeling activity. His-tagged Snf2H and Snf2L coupled to beads were used in remodeling reactions as described in *B*. Nucleosome remodeling activities of the recombinant ATPases were significantly reduced (lanes 1–6) and comparable to the activity of the purified GFP-tagged, bead-bound Snf2H and Snf2L proteins (lanes 7–14). Similar protein levels were used and nucleosome remodeling was analyzed on 6% polyacrylamide gels. (*D*) The activities of the three Snf2L ATPases (His-Snf2L, GFP-Snf2L, and GFP-Snf2L+13) were compared on the nucleosomal 601 DNA, placing the nucleosome at the border of a 208-bp-long DNA fragment (lanes 1, 5, and 9). The 601 nucleosome was incubated with the indicated remodelers in the absence or the presence of ATP and the remodeling reaction was analyzed as in *C*.

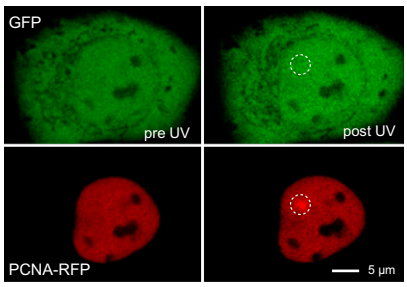

Fig. S4. GFP control for microirradiation experiments. Confocal images of the distribution of the isolated GFP protein are shown for the case of DNA damage. No GFP enrichment was observed at the DNA repair site where PCNA accumulated.

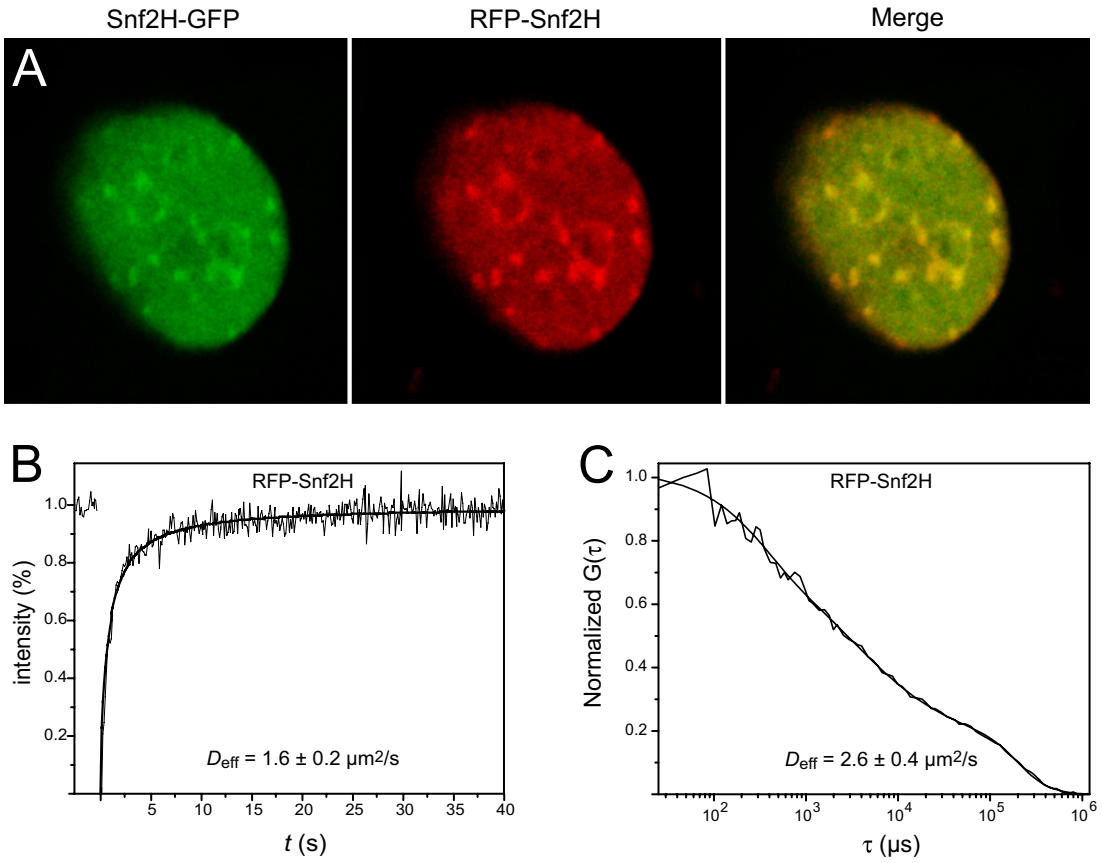

Fig. S5. RFP-Snf2H and Snf2H-GFP were indistinguishable. To verify that the GFP tag did not have a strong impact on Snf2H localization or dynamics, RFP-Snf2H was compared with Snf2H-GFP. (*A*) RFP-Snf2H and Snf2H-GFP colocalized in murine 3T3 cells. (*B*) RFP-Snf2H displayed an effective diffusion behavior in FRAP experiments, and virtually no immobile fraction was detected. (*C*) RFP-Snf2H behaved similarly to Snf2H-GFP in FCS experiments; for small lag times subtle differences between the autocorrelation functions of GFP- or RFP-tagged Snf2H were present, which arise from different photophysics (dark states in TagRFP).

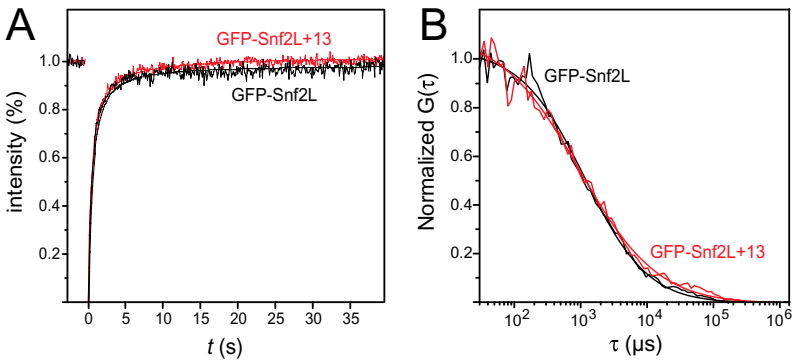

Fig. S6. Snf2H-GFP and GFP-Snf2L behave in HEK293T cells as in U2OS cells. The dynamics of GFP-Snf2L and GFP-Snf2L+13 were analyzed in HEK293T cells using FRAP (*A*) and FCS (*B*). In contrast to U2OS cells, HEK293T cells express active Snf2L. The two proteins displayed the same mobility in the two cell lines.

Table S1. Nuclear concentrations of GFP-tagged and endogenous proteins in U2OS cells

Protein	GFP-tagged protein, μM	Ratio GFP-tagged/ endogenous protein	Endogenous protein, μM
Snf2H-GFP	2.0 ± 0.1	2.4 ± 0.3	0.83 ± 0.13
GFP-Snf2L	0.5 ± 0.1	>10	<0.05
GFP-Snf2L+13	0.25 ± 0.05	1.8 ± 0.1	0.14 ± 0.04

Concentrations of GFP-tagged remodelers in the nucleus of stably transfected U2OS lines were measured by FCS. The ratios between the amount of endogenous and GFP-tagged proteins were determined by Western blotting and used to calculate the endogenous protein concentration in the nucleus. The value for Snf2L is the ratio between GFP-Snf2L and all endogenous Snf2L variants. The latter one was determined in the Snf2L+13-expressing U2OS cell line according to the following approach: The ratio of GFP-Snf2L+13 to endogenous Snf2L+13 (using an antibody against Snf2L+13) as well as the ratio between GFP-Snf2L+13 and all endogenous Snf2L variants was determined. Both ratios amounted to 1.8 ± 0.1, demonstrating that concentrations of endogenous Snf2L are negligible in the U2OS cell line. Thus, for the cell line stably expressing GFP-Snf2L the measured ratio reflects the concentration of GFP-Snf2L in relation to endogenous Snf2L+13.

Table S2. Dynamic parameters and sampling times for different ISWI-type remodelers

	Snf2H	Acf1/ACF	Snf2L
C, μM	0.83 ± 0.13	>0.15 ± 0.03	<0.05
k_{off}, s^{-1}	13.6 ± 2.3	2.3 ± 0.8	8.3 ± 1.5
t_{res}, ms	74 ± 12	430 ± 151	120 ± 22
K^*_{bin}	2.3 ± 0.7	2.0 ± 0.6	1.0 ± 0.3
$\tau_{sample,min}$, min:s	0:18 ± 0:04	<10:11 ± 4:12	>11:15 ± 2:39
$\tau_{sample,99\%}$, min:s	1:22 ± 0.18	<46:42 ± 19:16	>51:47 ± 12:12

Measured concentrations, dissociation rates, residence times, and pseudoaffinities were used to calculate the sampling times $\tau_{sample,\,min}$ and $\tau_{sample,\,99\%}$ for the different ISWI complex compounds as described in *SI Materials and Methods*. The parameter $\tau_{sample,\,99\%}$ is the average time it takes for a given protein to sample 99% of all genomic nucleosomes. For $\tau_{sample,\,min}$ the calculated coverage would correspond to 63%. t_{res} values determined from FRAP represent upper limits with the lower limit inferred from the FCS analysis being ~10 ms.